Spin Current as a Probe of the $\mathbb{Z}_2$-Vortex Topological Transition in the Classical Heisenberg Antiferromagnet on the Triangular Lattice

K. Aoyama and H. Kawamura
Department of Earth and Space Science, Graduate School of Science, Osaka University, Osaka 560-0043, Japan

(Received 18 September 2019; published 29 January 2020)

We have theoretically investigated transport properties of the classical Heisenberg antiferromagnet on the triangular lattice, in which a binding-unbinding topological transition of $\mathbb{Z}_2$ vortices is predicted to occur at a finite temperature T_v. It is shown by means of the hybrid Monte Carlo and spin-dynamics simulations that the longitudinal spin-current conductivity exhibits a divergence at T_v, while the thermal conductivity only shows a monotonic temperature dependence with no clear anomaly at T_v. The significant enhancement of the spin-current conductivity is found to be due to the rapid growth of the spin-current-relaxation time toward T_v, which can be understood as a manifestation of the topological nature of the free $\mathbb{Z}_2$ vortex whose lifetime gets longer toward T_v. The result suggests that the spin-current measurement is a promising probe to detect the $\mathbb{Z}_2$-vortex topological transition, which has remained elusive in experiments.

DOI: 10.1103/PhysRevLett.124.047202

In frustrated magnets, competitions between exchange interactions often result in a noncollinear magnetic state whose ordering wave vector may be commensurate or incommensurate with the underlying lattice structure. In the case of isotropic Heisenberg spins, such a noncollinear spin structure is invariant under any rotation in the three-dimensional spin space, so that the order parameter space has the topology of SO(3). On the two-dimensional lattice, a point defect, namely, a vortex excitation, in the SO(3) manifold is characterized by the topological number of $\mathbb{Z}_2$, and thus it is called a "$\mathbb{Z}_2$ vortex" [1]. In contrast to an ordinary vortex having an integer topological number $\mathbb{Z}$, less is known about how the $\mathbb{Z}_2$ vortices affect magnetic properties of the system. In this Letter, as a typical platform for the $\mathbb{Z}_2$ vortex, we consider the classical Heisenberg antiferromagnet on the triangular lattice and investigate its transport properties, focusing on the role of the $\mathbb{Z}_2$-vortex excitations.

The ground state of the triangular-lattice Heisenberg antiferromagnet with the nearest-neighbor (NN) exchange interaction J [1–5] is the noncollinear 120° Néel state, in which three spins on each triangle, $\mathbf{S}_1$, $\mathbf{S}_2$, and $\mathbf{S}_3$, constitute additional degrees of freedom, a chirality vector $\kappa = [2/(3\sqrt{3})](\mathbf{S}_1 \times \mathbf{S}_2 + \mathbf{S}_2 \times \mathbf{S}_3 + \mathbf{S}_3 \times \mathbf{S}_1)$. When the spin correlation develops over a lattice spacing at moderately high temperatures, the 120° spin structure is held in spatially local regions, e.g., elementary triangles. Such triangles having the local 120° structure and the associated chirality vector κ are building blocks of the $\mathbb{Z}_2$ vortex [1]. A typical $\mathbb{Z}_2$ vortex is shown in Fig. 1(a). In the three-component spin space, it forms a three-dimensionally oriented spin texture and can be viewed as a vortex formed by κ. The topological object of the $\mathbb{Z}_2$ vortex is relevant to the phase transition in this system [1–5].

As is well established, spins in the present system do not order except at $T = 0$. In other words, the spin correlation length ξ_s is finite at any finite temperature. In the middle 1980s, Kawamura and Miyashita theoretically predicted that, although spins are disordered with ξ_s being finite, there exists a Kosterlitz-Thouless (KT)-type topological phase transition associated with binding-unbinding of the $\mathbb{Z}_2$ vortices [1]. The $\mathbb{Z}_2$-vortex transition temperature T_v is estimated to be $T_v/|J| \simeq 0.285$ via extensive Monte Carlo (MC) simulations [4]. At lower temperatures $T < T_v$, all the $\mathbb{Z}_2$ vortices are paired up [see Fig. 1(b)], while at higher temperatures $T > T_v$, dissociated free $\mathbb{Z}_2$ vortices can be found [see Fig. 1(c)]. On approaching T_v from above, the vortex density is reduced due to the vortex-pair annihilation and, correspondingly, the vortex correlation length ξ_v, which corresponds to the distance between *free* vortices, diverges toward T_v, whereas the spin correlation length ξ_s remains finite [4,5]. Once across T_v, the ergodicity is broken, since the phase space is restricted only in the sector without free vortices. The low-temperature phase separated topologically from the ergodic disordered phase is sometimes called a "spin-gel" state [4–6].

In the triangular-lattice antiferromagnets $NiGa_2S_4$ [7–18], $FeGa_2S_4$ [19,20], $NaCrO_2$ [21–24], $KCrO_2$ [25,26], and $AAg_2Cr[VO_4]_2$ (A = K, Rb) [27], a long-range magnetic order has not been observed down to the lowest temperature reachable in experiments, indicating the realization of the spin-gel state, and the possible existence of the $\mathbb{Z}_2$-vortex transition has extensively been discussed. Nevertheless, the $\mathbb{Z}_2$-vortex transition has remained elusive because static physical quantities such as the specific heat C and the magnetic susceptibility χ_m exhibit only a weak essential singularity at T_v [4,5]. In this Letter, to propose a smoking-gun experiment to detect the transition, we examine

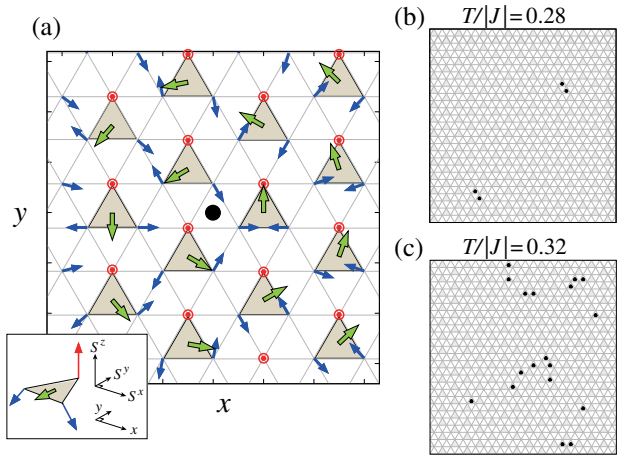

FIG. 1. (a) A schematically drawn $\mathbb{Z}_2$ vortex. Spin and chirality vectors projected onto the two-dimensional lattice (xy) plane, where the central black dot represents a vortex core. (Inset) An enlarged three-dimensional view of each gray-colored triangle in (a), where a red (blue) arrow represents a spin vector $\mathbf{S}_i$ pointing upward (downward) without (with) in-plane components, and a green one represents a chirality vector $\boldsymbol{\kappa}$. As the three spins at each gray-colored triangle constitute the 120° structure, $\boldsymbol{\kappa}$ does not have an out-of-plane component. Snapshots of the vortex-core distribution taken in the MC simulation below and above the $\mathbb{Z}_2$-vortex transition temperature $T_v/|J| = 0.285$ are shown in (b) and (c), respectively, where black dots represent vortex cores. The definition of the $\mathbb{Z}_2$-vortex core is the same as that in Ref. [1].

dynamical physical quantities that may sensitively capture the dynamics characteristic of bound and unbound vortices. In this context, it was theoretically pointed out that the paired and free vortices show different characteristic features in the dynamical spin structure factor near M and K points of the Brillouin zone, respectively [6]. Since, in general, dynamical properties should also be reflected in transport phenomena, here, we theoretically investigate the conductivity of spin and thermal currents, putting particular emphasis on the spin transport, which is nowadays becoming available as a probe to study magnetic fluctuations and excitations [28–34].

In the low-temperature phase (spin-gel state) below T_v, spin and thermal currents should be carried by spin waves or magnons. At higher temperatures above T_v, thermally activated free $\mathbb{Z}_2$ vortices may strongly affect the current relaxation, because the vortex as a topological object is generally robust against perturbations, resulting in a relatively long lifetime compared with the damping of the spin-wave mode. As we will demonstrate in this Letter, this is actually the case for the spin-current relaxation, which gets slower on cooling toward T_v, and as a result, the longitudinal spin-current conductivity grows up to diverge at T_v, serving as a distinct probe of the $\mathbb{Z}_2$-vortex transition.

The model Hamiltonian we consider is given by

$$\mathcal{H} = -J\sum_{\langle i,j\rangle}\mathbf{S}_i \cdot \mathbf{S}_j, \tag{1}$$

and its dynamical properties is determined by the semiclassical equation of motion,

$$\frac{d\mathbf{S}_i}{dt} = \mathbf{S}_i \times J\sum_{j\in N(i)}\mathbf{S}_j, \tag{2}$$

where $\mathbf{S}_i$ is a classical Heisenberg spin, $J < 0$, $\langle i,j\rangle$ denotes the summation over all the NN pairs, and $N(i)$ denotes all the NN sites of i. Since Eq. (2) is a classical analog of the Heisenberg equation for the spin operator, all the static and dynamical magnetic properties intrinsic to the Hamiltonian (1) should be described by the combined use of Eqs. (1) and (2). From the conservation of the magnetization and the energy, one can define the spin current $\mathbf{J}_s^\alpha$ and the thermal current $\mathbf{J}_{\rm th}$ as follows [35–45]:

$$\mathbf{J}_s^\alpha = J\sum_{\langle i,j\rangle}(\mathbf{r}_i - \mathbf{r}_j)(\mathbf{S}_i \times \mathbf{S}_j)^\alpha, \tag{3}$$

$$\mathbf{J}_{\rm th} = \frac{J^2}{4}\sum_i \sum_{j,k\in N(i)}(\mathbf{r}_j - \mathbf{r}_k)(\mathbf{S}_j \times \mathbf{S}_k)\cdot \mathbf{S}_i, \tag{4}$$

where α in $\mathbf{J}_s^\alpha$ denotes the spin component. One can see from Eqs. (3) and (4) that $\mathbf{J}_s^\alpha$ and $\mathbf{J}_{\rm th}$ are associated with the vector and scalar chiralities, respectively. Since the $\mathbb{Z}_2$ vortex is a texture formed by the vector chirality κ, the spin transport is expected to be sensitive to the existence of the $\mathbb{Z}_2$ vortex.

Within the linear response theory [46], one can define the spin-current conductivity $\sigma_{\mu\nu}^s$ and the thermal conductivity $\kappa_{\mu\nu}$ for the classical spin systems as follows [36–38,40,41,45]:

$$\sigma_{\mu\nu}^s = \frac{1}{TL^2}\int_0^\infty dt\langle J_{s,\nu}(0)J_{s,\mu}(t)\rangle,$$
$$\langle J_{s,\nu}(0)J_{s,\mu}(t)\rangle = \frac{1}{3}\sum_{\alpha=x,y,z}\langle J_{s,\nu}^\alpha(0)J_{s,\mu}^\alpha(t)\rangle, \tag{5}$$

$$\kappa_{\mu\nu} = \frac{1}{T^2L^2}\int_0^\infty dt\langle J_{{\rm th},\nu}(0)J_{{\rm th},\mu}(t)\rangle, \tag{6}$$

where L is a linear system size, $\langle O\rangle$ denotes the thermal average of a physical quantity O, and the spin-current conductivity $\sigma_{\mu\nu}^s$ is averaged over the three spin components because the spin space is isotropic in the present Heisenberg model. Noting that, in Eq. (2), time t is measured in units of $|J|^{-1}$, it turns out that $\sigma_{\mu\nu}^s$ is a dimensionless quantity and $\kappa_{\mu\nu}$ has the dimension of $|J|$. As we take the lattice constant a to be $a = 1$, the total number of spin $N_{\rm spin}$ and L is related by $N_{\rm spin} = L^2$.

In Eqs. (3) and (4), the time evolutions of $\mathbf{J}_s^\alpha$ and $\mathbf{J}_{\rm th}$ are determined microscopically by the spin-dynamics equation (2). By using the second-order symplectic method [6,47,48], we numerically integrate Eq. (2) typically up to

$t = 100|J|^{-1}$–$800|J|^{-1}$ with the time step $\delta t = 0.01|J|^{-1}$ and initial spin configurations generated by MC simulations. In this Letter, we performed 10–20 independent MC runs starting from different initial configurations under the periodic boundary conditions, and prepared 2000–4000 equilibrium spin configurations by picking up a spin snapshot every 1000 MC sweeps after 10^5 MC sweeps for thermalization, where one MC sweep consists of one heat-bath sweep and successive 10–30 over-relaxation sweeps. The thermal average is taken as the average over initial equilibrium spin configurations. We have checked that results are not altered if the fourth-order Runge-Kutta method is used instead of the second-order symplectic method. By analyzing the system-size dependence of $\sigma^s_{\mu\nu}$ and $\kappa_{\mu\nu}$, we will discuss the temperature dependences of the conductivities in the thermodynamic limit ($L \to \infty$) of our interest.

Figure 2 shows the longitudinal (xx) and transverse (yx) components of the spin-current conductivity $\sigma^s_{\mu\nu}$ and the thermal conductivity $\kappa_{\mu\nu}$ as a function of the temperature T, which are obtained for various system sizes ranging from $L = 24$ to $L = 768$. Since the result on the yy (xy) component is qualitatively the same as that on the xx (yx) one, only the latter is shown in Fig. 2, where the x and y directions are taken along the bond and off-bond directions of the triangular lattice, respectively [see Fig. 1(a)]. As readily seen from Fig. 2, the longitudinal spin-current conductivity σ^s_{xx} exhibits a divergent sharp peak near T_v, while the longitudinal thermal conductivity κ_{xx} only shows a monotonic temperature dependence, except for a possible weak anomaly near T_v, which is, however, not evident at the precision of our numerical calculation. In both the spin and thermal transports, the transverse Hall response, σ^s_{yx} and κ_{yx}, is absent at 2σ precision [see Fig. 2(c)].

We first discuss the low-temperature transport caused by magnons, which might be described by the linear-spin-wave theory (LSWT). As shown in Fig. 2(b), κ_{xx} increases monotonically toward $T = 0$. As LSWT predicts $\kappa_{xx} \propto 1/\alpha_d$ with the magnon damping α_d (see Supplemental Material [49]), the observed monotonic increase in κ_{xx} can be understood as a result of the reduced scattering rate of magnons toward $T = 0$, i.e., $\alpha_d \to 0$ [45]. Since the spin current should be carried by magnons as well, one may naively expect that σ^s_{xx} increases toward $T = 0$ similar to κ_{xx}, but this does not seem to be the case for the numerically obtained σ^s_{xx} [see Fig. 2(a)]. Also, in LSWT, the magnon-spin-current conductivity is calculated as $\sigma^s_{xx} \sim \mathrm{const}T/\alpha_d + T\alpha_d\xi_s$ with $\xi_s \sim \exp[b_H|J|/T]$ [49], suggesting that its temperature dependence is not so trivial because of the competition between $\alpha_d \to 0$ and $\xi_s \to \infty$. Such a situation is in sharp contrast to that of the unfrustrated Heisenberg antiferromagnet on the square lattice, in which $\sigma^s_{xx} \sim \mathrm{const}T/\alpha_d + T\xi_s/\alpha_d$ is obtained, i.e., σ^s_{xx} unambiguously increases in a monotonic manner toward $T = 0$. This increasing behavior has been confirmed by numerical simulations [45]. In the present system, although the $T \to 0$ limit of σ^s_{xx} remains unclarified, at least it is certain that the unusual low-temperature spin transport has its origin in the magnetic frustration.

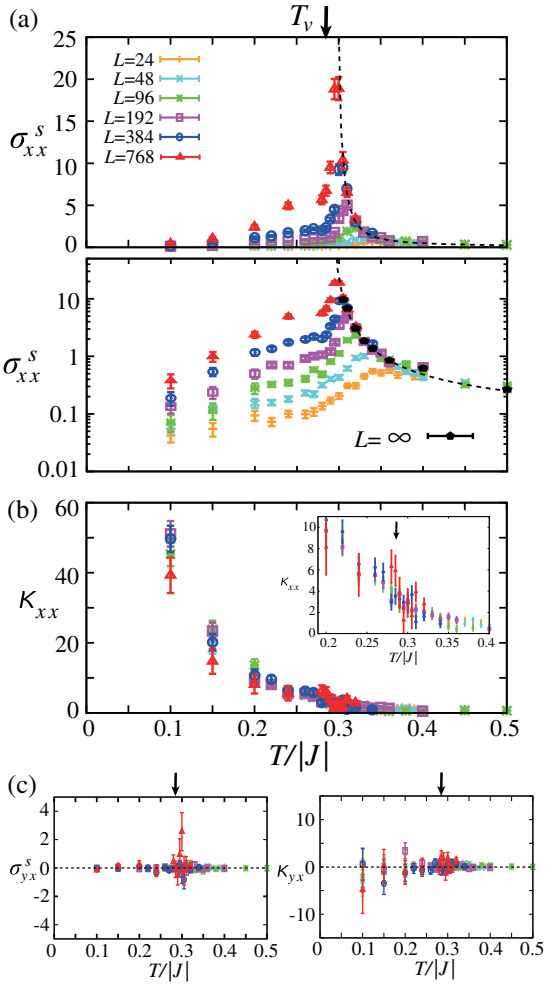

FIG. 2. The temperature dependence of the spin-current conductivity $\sigma^s_{\mu\nu}$ and the thermal conductivity $\kappa_{\mu\nu}$, where the longitudinal (transverse) components of $\sigma^s_{\mu\nu}$ and $\kappa_{\mu\nu}$ are shown in (a) [(c), left] and (b) [(c), right], respectively. $\kappa_{\mu\nu}$ is measured in units of $|J|$, whereas $\sigma^s_{\mu\nu}$ is a dimensionless quantity. A black arrow indicates the $\mathbb{Z}_2$-vortex transition temperature, $T_v/|J| \simeq 0.285$. In (a), the lower panel shows a semilogarithmic plot of the upper panel together with black-colored data representing σ^s_{xx} values in the thermodynamic limit of $L \to \infty$, and a dashed curve represents the $\sigma^s_{xx}(T)$ curve obtained by fitting the $L \to \infty$ data (see the main text). In (b), the inset shows an enlarged view near T_v.

Next, we discuss the significant enhancement of σ^s_{xx} near T_v, which points to a strong association between the spin transport and the $\mathbb{Z}_2$-vortex transition. As one can clearly see from the lower panel of Fig. 2(a), with increasing the system size L, the peak height in σ^s_{xx} increases and the peak temperature approaches $T_v/|J| \simeq 0.285$ from above, suggesting that, in the $L \to \infty$ limit, σ^s_{xx} diverges at T_v. At $T \gtrsim 0.3|J| > T_v$, σ^s_{xx} saturates to a constant value as a function of the system size L which corresponds to σ^s_{xx} in

the thermodynamic limit of $L \to \infty$. The $L \to \infty$ values of σ^s_{xx} are represented by black symbols in the lower panel of Fig. 2(a).

Now, we discuss the functional form characterizing the divergence of σ^s_{xx} at T_v. Noting that the vortex correlation length ξ_v grows up toward T_v in the exponential form $\xi_v \sim \exp\{A[|J|/(T-T_v)]^\alpha\}$ with the estimated values of $\alpha = 0.42$ and $A = 0.84$–0.97 [4], we fit the $L \to \infty$ data of σ^s_{xx} with the functional form of $b\exp\{a[|J|/(T-T_v)]^{0.42}\}$. The resultant fitting function with the obtained values of $a = 1.15 \pm 0.06$ and $b = 0.028 \pm 0.007$ is represented by a dashed curve in Fig. 2(a). One can see that the obtained exponential form well characterizes the divergent behavior of σ^s_{xx}.

To clarify the origin of the exponential divergence, we examine the temperature dependence of the time correlation function $\langle J_{s,x}(0)J_{s,x}(t)\rangle$, which involves the fundamental information about σ^s_{xx} [see Eq. (5)]. The inset of Fig. 3(a) shows a typical example of the time correlation function normalized by the system size $\langle j_{s,x}(0)j_{s,x}(t)\rangle \equiv \langle J_{s,x}(0)J_{s,x}(t)\rangle/L^2$. As the time correlation decays exponentially in the form of $\exp[-t/\tau_s]$, one can define a characteristic timescale, namely, a spin-current-relaxation time τ_s. Then, the time correlation function can roughly be written as $\langle j_{s,x}(0)j_{s,x}(t)\rangle \sim \langle |j_{s,x}(0)|^2\rangle \exp[-t/\tau_s]$. By carrying out the integral over time in Eq. (5), one can estimate the longitudinal spin-current conductivity as $\sigma^s_{xx} \sim T^{-1}\tau_s\langle |j_{s,x}(0)|^2\rangle$. Figure 3 shows the temperature dependences of $\langle |j_{s,x}(0)|^2\rangle$ and τ_s, where τ_s is extracted by

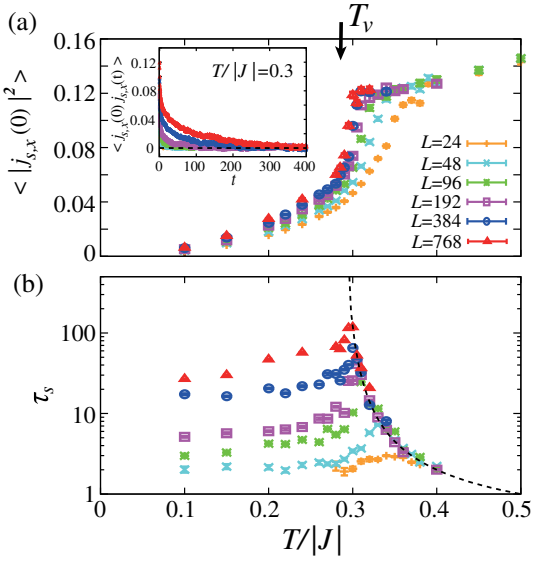

FIG. 3. The temperature dependence of the (a) equal-time spin-current correlation $\langle |j_{s,x}(0)|^2\rangle$ and the (b) spin-current-relaxation time τ_s, which are measured in units of $|J|^2$ and $|J|^{-1}$, respectively. A black arrow indicates T_v and a dashed curve in (b) represents an exponential function obtained by fitting the data above T_v (see the main text). The inset of (a) shows the time correlation function of the spin current $\langle j_{s,x}(0)j_{s,x}(t)\rangle$ at $T/|J| = 0.3$.

fitting the long-time tail of $\langle j_{s,x}(0)j_{s,x}(t)\rangle$ with $\exp[-t/\tau_s]$. One can see that on approaching T_v from above, τ_s is significantly enhanced, while $\langle |j_{s,x}(0)|^2\rangle$ exhibits a weaker anomaly. The functional type characterizing the steep increase in τ_s is also an exponential one. By fitting the data at $T/|J| \gtrsim 0.3$ with $\tilde{b}\exp\{\tilde{a}[|J|/(T-T_v)]^{0.42}\}$, we obtain $\tilde{a} = 1.21 \pm 0.05$ and $\tilde{b} = 0.10 \pm 0.02$. The extrapolated $\tau_s(T)$ curve represented by a dashed curve in Fig. 3(b) well characterizes the numerically obtained divergent behavior of τ_s. As σ^s_{xx} is related to τ_s and $\langle |j_{s,x}(0)|^2\rangle$ via $\sigma^s_{xx} \sim T^{-1}\tau_s\langle |j_{s,x}(0)|^2\rangle$, it turns out that the divergent behavior in σ^s_{xx} originates from the exponential rapid growth of τ_s toward T_v. Actually, the obtained values of a and $\tilde{a}$ are close to each other.

Here, we provide the physical interpretation of the above result. On cooling toward T_v, the inter-free-vortex distance ξ_v increases, so that a free $\mathbb{Z}_2$ vortex wanders for a longer time until it collides with an other free $\mathbb{Z}_2$ vortex to be pair annihilated. Since the vortex motion is not ballistic but rather diffusive [49], the vortex lifetime τ_v could be estimated roughly as $\tau_v \propto \xi_v^2 \sim \exp\{2A[|J|/(T-T_v)]^\alpha\}$, so that τ_v should get longer in the exponential form toward T_v with $2A \simeq 1.68$–1.94, which is comparable to a and $\tilde{a}$. Since the two timescales τ_s and τ_v develop toward T_v in almost the same manner as a function of the temperature and, furthermore, σ^s_{xx} is proportional to τ_s, we could conclude that the divergent peak at T_v in the σ^s_{xx} curve is attributed to the topological excitations of the long-lifetime free $\mathbb{Z}_2$ vortices.

Finally, we address experimental aspects to detect the divergent enhancement of $\sigma^s_{\mu\mu}$ at T_v. Since a single crystal is necessary for transport experiments, a good candidate material in this respect would be $NiGa_2S_4$ [7–18]. In the antiferromagnetic insulator $NiGa_2S_4$, although spins do not order down to the lowest temperature, a weak but clear transitionlike anomaly, which may be attributed to the binding-unbinding of the $\mathbb{Z}_2$ vortices, has been observed at T^* slightly below the specific-heat broad peak temperature. When the nonlocal measurement of the spin current [61–63] is done on $NiGa_2S_4$, it is expected that a significant enhancement of $\sigma^s_{\mu\mu}$, i.e., a gigantic signal in the inverse spin Hall detector or a very-long-distance transport of spin information, would be observed at T^* as distinct evidence for the $\mathbb{Z}_2$-vortex transition (see Supplemental Material [49]). We emphasize that only $\sigma^s_{\mu\mu}$ diverges at T_v, while the static quantities C and χ_m do not, which is in contrast to a ferromagnet where C and χ_m as well as $\sigma^s_{\mu\mu}$ exhibit critical behaviors at the transition [41,64–66]. Such a characteristic spin-transport phenomenon may be observed also in $FeGa_2S_4$ [19,20], $NaCrO_2$ [21–24], and $KCrO_2$ [25,26], in which a putative $\mathbb{Z}_2$-vortex anomaly has been reported, so that further experimental study including single-crystal growth on these compounds is strongly awaited. We note that, in the present system with finite ξ_s, perturbative

interactions including magnetic anisotropy D and the interlayer coupling J'_{3D}, which may exist in real materials, are irrelevant as long as their effective energy scale, e.g., $D(J'_{3D})\xi_s^2$, is smaller than $k_B T_v$, while in the KT transition, ξ_s diverges and, thereby, they become inevitably relevant [45].

In conclusion, we have theoretically shown that, in the Heisenberg antiferromagnet on the triangular lattice, the longitudinal spin-current conductivity exhibits a divergence at the temperature of the $\mathbb{Z}_2$-vortex binding-unbinding topological transition. Such a significant enhancement of the spin transport is smoking-gun experimental evidence for the so-far elusive $\mathbb{Z}_2$-vortex transition, which can potentially exist in a large variety of two-dimensional Heisenberg magnets possessing noncollinear spin correlations.

The authors thank K. Uematsu, S. Furuya, H. Adachi, and Y. Niimi for useful discussions. We are thankful to ISSP, the University of Tokyo, and YITP, Kyoto University for providing us with CPU time. This work is supported by JSPS KAKENHI Grants No. JP16K17748 and No. JP17H06137.

[1] H. Kawamura and S. Miyashita, J. Phys. Soc. Jpn. **53**, 4138 (1984).
[2] B. W. Southern and H.-J. Xu, Phys. Rev. B **52**, R3836 (1995).
[3] M. Wintel, H. U. Everts, and W. Apel, Phys. Rev. B **52**, 13480 (1995).
[4] H. Kawamura, A. Yamamoto, and T. Okubo, J. Phys. Soc. Jpn. **79**, 023701 (2010).
[5] H. Kawamura, J. Phys. Conf. Ser. **320**, 012002 (2011).
[6] T. Okubo and H. Kawamura, J. Soc. Phys. Jpn. **79**, 084706 (2010).
[7] S. Nakatsuji, Y. Nambu, H. Tonomura, O. Sakai, S. Jonas, C. Broholm, H. Tsunetsugu, Y. Qiu, and Y. Maeno, Science **309**, 1697 (2005).
[8] Y. Nambu, S. Nakatsuji, and Y. Maeno, J. Phys. Soc. Jpn. **75**, 043711 (2006).
[9] Y. Nambu, S. Nakatsuji, Y. Maeno, E. K. Okudzeto, and J. Y. Chan, Phys. Rev. Lett. **101**, 207204 (2008).
[10] H. Takeya, K. Ishida, K. Kitagawa, Y. Ihara, K. Onuma, Y. Maeno, Y. Nambu, S. Nakatsuji, D. E. MacLaughlin, A. Koda, and R. Kadono, Phys. Rev. B **77**, 054429 (2008).
[11] D. E. MacLaughlin, Y. Nambu, S. Nakatsuji, R. H. Heffner, L. Shu, O. O. Bernal, and K. Ishida, Phys. Rev. B **78**, 220403(R) (2008).
[12] A. Yaouanc, P. Dalmas de Reotier, Y. Chapuis, C. Marin, G. Lapertot, A. Cervellino, and A. Amato, Phys. Rev. B **77**, 092403 (2008).
[13] H. Yamaguchi, S. Kimura, M. Hagiwara, Y. Nambu, S. Nakatsuji, Y. Maeno, and K. Kindo, Phys. Rev. B **78**, 180404(R) (2008).
[14] H. Yamaguchi, S. Kimura, M. Hagiwara, Y. Nambu, S. Nakatsuji, Y. Maeno, A. Matsuo, and K. Kindo, J. Phys. Soc. Jpn. **79**, 054710 (2010).
[15] S. Nakatsuji, Y. Nambu, and S. Onoda, J. Phys. Soc. Jpn. **79**, 011003 (2010).
[16] Y. Nambu and S. Nakatsuji, J. Phys. Condens. Matter **23**, 164202 (2011).
[17] C. Stock, S. Jonas, C. Broholm, S. Nakatsuji, Y. Nambu, K. Onuma, Y. Maeno, and J.-H. Chung, Phys. Rev. Lett. **105**, 037402 (2010).
[18] Y. Nambu, J. S. Gardner, D. E. MacLaughlin, C. Stock, H. Endo, S. Jonas, T. J. Sato, S. Nakatsuji, and C. Broholm, Phys. Rev. Lett. **115**, 127202 (2015).
[19] Songrui Zhao, P. Dalmas de Reotier, A. Yaouanc, D. E. MacLaughlin, J. M. Mackie, O. O. Bernal, Y. Nambu, T. Higo, and S. Nakatsuji, Phys. Rev. B **86**, 064435 (2012).
[20] P. Dalmas de Reotier, A. Yaouanc, D. E. MacLaughlin, Songrui Zhao, T. Higo, S. Nakatsuji, Y. Nambu, C. Marin, G. Lapertot, A. Amato, and C. Baines, Phys. Rev. B **85**, 140407(R) (2012).
[21] A. Olariu, P. Mendels, F. Bert, B. G. Ueland, P. Schiffer, R. F. Berger, and R. J. Cava, Phys. Rev. Lett. **97**, 167203 (2006).
[22] D. Hsieh, D. Qian, R. F. Berger, R. J. Cava, J. W. Lynn, Q. Huang, and M. Z. Hasan, Physica (Amsterdam) **403B**, 1341 (2008).
[23] D. Hsieh, D. Qian, R. F. Berger, R. J. Cava, J. W. Lynn, Q. Huang, and M. Z. Hasan, J. Phys. Chem. Solids **69**, 3174 (2008).
[24] M. Hemmida, H. A. Krug von Nidda, N. Buttgen, A. Loidl, L. K. Alexander, R. Nath, A. V. Mahajan, R. F. Berger, R. J. Cava, Yogesh Singh, and D. C. Johnston, Phys. Rev. B **80**, 054406 (2009).
[25] J. L. Soubeyroux, D. Fruchart, C. Delmas, and G. Le. Flem, J. Magn. Magn. Mater. **14**, 159 (1979).
[26] F. Xiao, T. Lancaster, P. J. Baker, F. L. Pratt, S. J. Blundell, J. S. Moller, N. Z. Ali, and M. Jansen, Phys. Rev. B **88**, 180401(R) (2013).
[27] J. Tapp, C. R. dela Cruz, M. Bratsch, N. E. Amuneke, L. Postulka, B. Wolf, M. Lang, H. O. Jeschke, R. Valenti, P. Lemmens, and A. Moller, Phys. Rev. B **96**, 064404 (2017).
[28] L. Frangou, S. Oyarzun, S. Auffret, L. Vila, S. Gambarelli, and V. Baltz, Phys. Rev. Lett. **116**, 077203 (2016).
[29] Z. Qiu, J. Li, D. Hou, E. Arenholz, A. T. N'Diaye, A. Tan, K. Uchida, K. Sato, S. Okamoto, Y. Tserkovnyak, Z. Q. Qiu, and E. Saitoh, Nat. Commun. **7**, 12670 (2016).
[30] H. Wang, D. Hou, Z. Qiu, T. Kikkawa, E. Saitoh, and X. Jin, J. Appl. Phys. **122**, 083907 (2017).
[31] L. Frangou, G. Forestier, S. Auffret, S. Gambarelli, and V. Baltz, Phys. Rev. B **95**, 054416 (2017).
[32] O. Gladii, L. Frangou, G. Forestier, R. L. Seeger, S. Auffret, I. Joumard, M. Rubio-Roy, S. Gambarelli, and V. Baltz, Phys. Rev. B **98**, 094422 (2018).
[33] Y. Ou, D. C. Ralph, and R. A. Buhrman, Phys. Rev. Lett. **120**, 097203 (2018).
[34] J. Li, Z. Shi, V. H. Ortiz, M. Aldosary, C. Chen, V. Aji, P. Wei, and J. Shi, Phys. Rev. Lett. **122**, 217204 (2019).
[35] N. A. Lurie, D. L. Huber, and M. Blume, Phys. Rev. B **9**, 2171 (1974).
[36] B. Jencic and P. Prelovsek, Phys. Rev. B **92**, 134305 (2015).
[37] A. Mook, J. Henk, and I. Mertig, Phys. Rev. B **94**, 174444 (2016).
[38] A. Mook, B. Gobel, J. Henk, and I. Mertig, Phys. Rev. B **95**, 020401(R) (2017).
[39] D. L. Huber, Prog. Theor. Phys. **39**, 1170 (1968).

[40] A. V. Savin, G. P. Tsironis, and X. Zotos, Phys. Rev. B **72**, 140402(R) (2005).
[41] K. Kawasaki, J. Phys. Chem. Solids **28**, 1277 (1967).
[42] M. Sentef, M. Kollar, and A. P. Kampf, Phys. Rev. B **75**, 214403 (2007).
[43] A. S. T. Pires and L. S. Lima, Phys. Rev. B **79**, 064401 (2009).
[44] Z. Chen, T. Datta, and D. Yao, Eur. Phys. J. B **86**, 63 (2013).
[45] K. Aoyama and H. Kawamura, Phys. Rev. B **100**, 144416 (2019).
[46] R. Kubo, J. Phys. Soc. Jpn. **12**, 570 (1957).
[47] M. Krech, A. Bunker, and D. P. Landau, Comput. Phys. Commun. **111**, 1 (1998).
[48] S. C. Furuya, M. Oshikawa, and I. Affleck, Phys. Rev. B **83**, 224417 (2011).
[49] See Supplemental Material at http://link.aps.org/supplemental/10.1103/PhysRevLett.124.047202 for the analytical calculation of the conductivity in LSWT, the numerical result on the diffusive motion of the $\mathbb{Z}_2$ vortex and the effect of the interface with the spin-Hall metal, which includes Refs. [50–60].
[50] A. M. Polyakov, Phys. Lett. **59B**, 79 (1975).
[51] S. Ty and B. I. Halperin, Phys. Rev. B **42**, 2096 (1990).
[52] A. V. Chubukov, S. Sachdev, and T. Senthil, J. Phys. Condens. Matter **6**, 8891 (1994).
[53] A. L. Chernyshev and M. E. Zhitomirsky, Phys. Rev. B **79**, 144416 (2009).
[54] A. A. Abrikosov, L. P. Gorkov, and I. E. Dzyaloshinski, *Methods of Quantum Field Theory in Statistical Physics* (Dover Publications, New York, 1963).
[55] T. Yamaguchi and H. Kohno, J. Phys. Soc. Jpn. **86**, 063706 (2017).
[56] G. Tatara, Phys. Rev. B **92**, 064405 (2015).
[57] A. B. Harris, D. Kumar, B. I. Halperin, and P. C. Hohenberg, Phys. Rev. B **3**, 961 (1971).
[58] S. Takahashi, E. Saitoh, and S. Maekawa, J. Phys. Conf. Ser. **200**, 062030 (2010).
[59] Y. Yamamoto, M. Ichioka, and H. Adachi, Phys. Rev. B **100**, 064419 (2019).
[60] S. M. Wu, J. E. Pearson, and A. Bhattacharya, Phys. Rev. Lett. **114**, 186602 (2015).
[61] Y. Kajiwara, K. Harii, S. Takahashi, J. Ohe, K. Uchida, M. Mizuguchi, H. Umezawa, H. Kawai, K. Ando, K. Takanashi, S. Maekawa, and E. Saitoh, Nature (London) **464**, 262 (2010).
[62] B. L. Giles, Z. Yang, J. S. Jamison, and R. C. Myers, Phys. Rev. B **92**, 224415 (2015).
[63] L. J. Cornelissen, J. Liu, R. A. Duine, J. Ben Youssef, and B. J. van Wees, Nat. Phys. **11**, 1022 (2015).
[64] H. S. Bennett and P. C. Martin, Phys. Rev. **138**, A608 (1965).
[65] K. Kawasaki, Prog. Theor. Phys. **39**, 1133 (1968).
[66] P. C. Hohenberg and B. I. Halperin, Rev. Mod. Phys. **49**, 435 (1977).